Hydraulic conditions at the source zone and their impact on plume behavior

Nils Gueting · Andreas Englert

Abstract A laboratory sandbox model (105×60×15cm) was filled with different types of sediments to arrange different hydraulic conditions at the tracer's injection zone. Tracer-input functions were monitored at the injection location and tracer breakthrough curves (BTCs) were measured at a downgradient detection plane. Numerical transport simulations analogous to the sandbox experiments were conducted in a numerical model parameterized with the properties of the sediments used in the sandbox. The results of the study demonstrate that the hydraulic conditions at the source zone have a major influence on plume development. Tracer injection into high-permeability zones causes early arrival, and enhanced transverse and reduced longitudinal spreading. Tracer injection into low-permeability zones causes late arrival, and reduced transverse and enhanced longitudinal spreading. It was further found that using simplified tracer-input functions in the analysis of BTCs can lead to biased transport parameters. The results suggest that transport parameter estimation based on tracer experiments can benefit from monitoring of the tracer-input function and subsequent consideration of the measured tracer-input function in the analysis of BTCs.

Keywords Heterogeneity · Laboratory experiments/measurements · Numerical modeling · Solute transport

Introduction

Environmental engineering procedures such as remediation of contaminated sites rely on precise prediction of flow and transport processes in the subsurface, which are controlled by the subsurface's chemical and physical heterogeneity. Among the various chemical and physical properties, the hydraulic conductivity is generally recognized as the primary control on groundwater flow and solute migration (e.g. Dagan 1989; Koltermann and Gorelick 1996). The spatial distribution of the hydraulic conductivity in aquifers has been extensively studied (e.g. Sudicky 1986; Hess 1989; Boggs et al. 1992; Vereecken et al. 2000). These studies showed that the local hydraulic conductivity in aquifers can vary over several orders of magnitude, with typical correlation lengths ranging from decimeters to meters. The spatial variability of the local hydraulic conductivity causes convergence and divergence of streamlines, which locally focuses and defocuses groundwater flow. The impact of heterogeneous flow fields on solute spreading and plume behavior is, as such, relatively well understood. Among many others, Silliman and Simpson (1987) investigated the influence of heterogeneity on solute transport and showed that the presence of heterogeneities significantly increases solute spreading and causes dispersion to scale with travel distance. Levy and Berkowitz (2003) demonstrated that heterogeneous structures strongly affect plume spreading and lead to irregularly shaped solute plumes. Werth et al. (2006) and Rolle et al. (2009) investigated the effect of 'flow focusing' through high-permeability inclusions and found that flow focusing enhances transverse mixing and therefore controls the lateral spreading of a plume and the length of a mixing-controlled reactive plume.

Although plume behavior in heterogeneous conductivity fields has been extensively studied, only a few studies investigated the influence of the hydraulic conditions at the source zone. Since the hydraulic conductivity in aquifers changes in space, the hydraulic conditions at a localized solute source can be very different at different locations within the aquifer, because they depend on the local hydraulic conductivity at the source zone relative to the surrounding conductivity field. De Barros and Nowak (2010) could show analytically and numerically that flow focusing/defocusing is of particular importance for plume development when it occurs directly at the source zone. The authors found the volumetric water flux passing through the source zone to control the ensemble characteristics of downgradient plumes. Their results are in alignment with the findings of Nowak et al. (2010), who identified the flow field at the source zone to be a major source of uncertainty in the prediction of contaminant

Received: 26 July 2012 / Accepted: 10 February 2013
Published online: 15 March 2013

N. Gueting (✉) · A. Englert
Hydrogeology Department,
Ruhr University Bochum,
Universitätsstraße 150, 44801 Bochum, Germany
e-mail: nils.gueting@rub.de
Tel.: +49-234-3223335
Fax: +49-234-3214120

 DOI 10.1007/s10040-013-0962-7

plumes. In their numerical study on optimal sampling design, Nowak et al. (2010) conclude that optimal sampling schemes should investigate the hydraulic conditions at the source zone because knowledge thereof can greatly reduce the uncertainty in predicted contaminant concentrations.

Solute transport in porous media can be characterized in terms of advective–dispersive transport parameters, which can be determined in tracer experiments. Typically, tracer is injected at one location into the aquifer and tracer breakthrough curves (BTCs) are measured at some other downgradient location. Apparent advective–dispersive transport parameters, the apparent velocity and the apparent dispersivity, are delineated from the tracer's mean arrival time and from the spreading of the BTC, respectively (e.g. Leibundgut et al. 2009). The impact of aquifer heterogeneity on BTCs and on apparent transport parameters derived from BTCs is generally well understood. Silliman and Simpson (1987) and Huang et al. (1995) analyzed BTCs in laboratory transport experiments and showed that heterogeneous structures increase the spreading of BTCs and lead to scale-dependent dispersivities obtained from BTCs. Levy and Berkowitz (2003) demonstrated that the presence of heterogeneities can produce anomalous transport characteristics such as non-Fickian early arrival and late-time tails in BTCs. What has not yet been studied in detail is the influence of the hydraulic conditions at the source zone on BTCs and on apparent transport parameters derived from BTCs. In the case of a tracer test where tracer is injected at a well, the hydraulic conditions at the injection well depend on the aquifer's hydraulic conductivity close to the well and farther away from the well. However, additionally to the natural heterogeneity of the aquifer, the well itself disturbs the flow field close to the well. Generally, streamlines converge in the vicinity of a borehole, which leads to an increased flow through the borehole compared to the undisturbed aquifer (Drost et al. 1968). Yet, depending on well construction and chemical conditions, processes such as formation of oxides/hydroxides or bacteria growth are known to clog the well screen or filter-pack which can dramatically decrease its hydraulic conductivity (van Beek et al. 2009).

Often, BTCs are interpreted assuming an instantaneous or a step pulse tracer-input profile. The use of such simplified approximations is appealing because it allows for use of simple analytical solutions in the analysis of BTCs. However, realistic experimental conditions may produce tracer-input functions that depart strongly from such approximations (Brouyère 2003). If not adequately considered, this can lead to severe misinterpretation of BTCs. Moench (1989) pointed out that well bore mixing in an injection well can induce a spreading of BTCs which must not be confused with the spreading due to aquifer dispersivity. Gelhar et al. (1992) recognized that the tailing of BTCs might stem from slow flushing of the input slug of tracer out of the injection borehole. Brouyère et al. (2005) demonstrated in synthetic experiments that erroneous transport parameters can be derived from BTCs when well-aquifer interactions during the injection are neglected.

The present study investigates the impact of different hydraulic conditions at the source zone on plume behavior by analyzing BTCs measured in laboratory tracer experiments. Different types of sediments were arranged in a sandbox model with dimensions x_1=105 cm, x_2=60 cm, x_3=15 cm to produce different hydraulic conditions at the tracer's source zone. Specific tracer-input functions were obtained through monitoring concentrations as a function of time at the location where tracer was injected. BTCs were measured at a downgradient detection plane and characterized in terms of apparent transport parameters, using temporal moment analyses and least-squares fits of the one-dimensional convection–dispersion equation (1-D CDE). Following the approach presented by Englert et al. (2007), the measured tracer-input functions were explicitly accounted for in the analysis of BTCs.

To understand in detail the spatio–temporal plume development, numerical transport simulations analogous to the sandbox experiments were conducted in a numerical model that was parameterized with the hydraulic properties of the sediments used in the sandbox.

The particular goals of the present study are (1) to explore the impact of different hydraulic conditions at the source zone on plume characteristics and BTCs measured at a downgradient detection plane, (2) to assess how much actual tracer-input functions deviate from commonly assumed instantaneous or step pulse injection profiles, (3) to investigate if transport parameter estimation based on BTC analysis can benefit from monitoring of the tracer-input function and subsequent consideration of the measured tracer-input function in the analysis of BTCs.

Materials and methods

Laboratory experiments

Experiments were conducted in a laboratory sandbox model. Figure 1 shows a sketch of the experimental setup. The sediment packing (grey area) is separated from an inlet chamber (left) and an outlet chamber (right) by screens, whose hydraulic conductivity is large relative to the hydraulic conductivity of the sediment. Two constant head reservoirs enforce steady flow from left to right. To establish parallel flow throughout the sediment packing, the water entering the inlet chamber is channeled through a vertical tube with equally spaced holes, and thus, distributed over the entire height of the model. Likewise, the water exiting the sediment packing is collected over the entire height by a similar tube in the outlet chamber. Two micropumps permanently circulate the water within the inlet chamber and the outlet chamber to enforce mixing.

Clean, sieved silica sediments were packed into the model. To avoid the trapping of air during the packing procedure, the sediments were initially put into a vessel and stirred with water until complete saturation was reached. Afterwards the saturated sediments were packed

 DOI 10.1007/s10040-013-0962-7

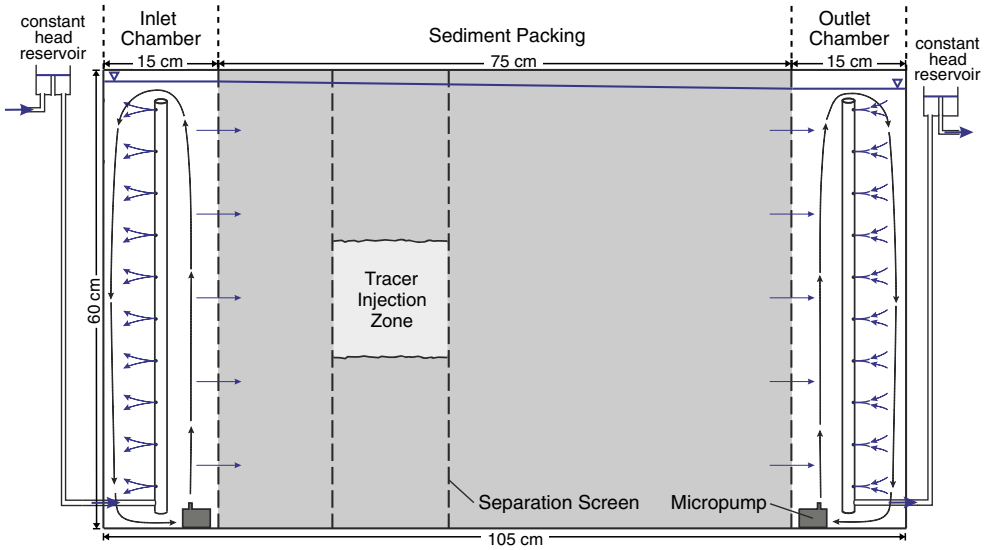

Fig. 1 Vertical cross-section of the laboratory model (thickness=15 cm)

into the model with the water level inside the model always being approximately 5 cm above the top of the sediment packing.

To minimize pore-clogging effects due to degassing of dissolved gases during the experiments, tap water was stored in a reservoir for at least 12 h, equilibrating with the laboratory air, before flowing through the model. Experiments were conducted at roughly constant air temperatures (18–21 °C), ascertaining a constant fluid viscosity.

Different types of sediments were used to arrange different hydraulic setups. In a first setup, the entire model was homogeneously filled with a sand of grain size 0.7–1.2 mm. Subsequently, the material within the injection zone (15×15×15 cm, light grey area in Fig. 1) was extracted and replaced by four other types of sediments which are characterized by coarser grain sizes (2.0–3.15 mm, 3.15–5.6 mm) or finer grain sizes (0.4–0.8 mm, 0.2–0.6 mm), respectively. The hydraulic conductivities of the different sediments were determined beforehand in Darcy experiments. Table 1 lists the resulting hydraulic conditions for the different injection zone setups. Note that for all setups, the initial sand-packing stayed in place at all other locations but the injection zone, that is, only the hydraulic properties of the injection zone are changed for the different setups.

Tracer experiments were repeated in the same manner for the five different setups. Potassium chloride solution was used as a tracer, so that tracer concentrations could be deduced from electrical conductivity (EC) measurements using calibration curves. The latter were obtained before and after each experiment using standard solutions. Using a syringe and a tube, a volume of 50-ml tracer solution was injected in a 20-s step pulse into a small filter element located in the middle of the injection zone (Fig. 2). The same filter element contained the measurement device of an EC sensor that was buried inside the sediment and connected to a logger, recording EC values with a temporal resolution of 5 s. This setup allows for measurement of the temporal evolution of tracer concentrations at the location where tracer was injected.

Further downstream, tracer concentrations were recorded in the outlet chamber by another EC sensor, recording EC values with a temporal resolution of 60 s. Preliminary experiments showed that the circulation pump, which permanently mixes the water within the outlet chamber, causes a slug injection of dye to be well mixed over the entire chamber volume within less than 30 s. Therefore, measurement of concentrations at one location within the chamber can be regarded to be representative for the entire chamber.

The tracer solution that was injected into the model had a concentration of c=0.3 mol/l. This relatively high concentration was chosen, because on the one hand, EC values measured in the outlet chamber must be sufficiently high above the tap water's background level and on the other hand, the volume of tracer solution that was injected must not largely exceed the

Table 1 Hydraulic conditions in the different setups

K [m/s][a] Injection zone ($K1$)	K [m/s][a] Surrounding material ($K2$)	$K1/K2$	Laboratory experiment	Numerical experiment
6.6E-04	6.1E-03	0.11	lp2	LP2
2.5E-03	6.1E-03	0.41	lp1	LP1
6.1E-03	6.1E-03	1.00	hm	HM
6.9E-03	6.1E-03	1.13	hp1	HP1
8.8E-03	6.1E-03	1.44	hp2	HP2
6.1E-02	6.1E-03	10.00	–	HP3[b]

hm/HM homogeneous setup; *lp/LP* low-permeable injection zone setup; *hp/HP* high-permeable injection zone setup

[a] Hydraulic conductivities (K) from Darcy experiments

[b] Additional numerical experiment to investigate the effects of a larger hydraulic contrast between a high-permeable injection zone and the surrounding material (no laboratory equivalent)

 DOI 10.1007/s10040-013-0962-7

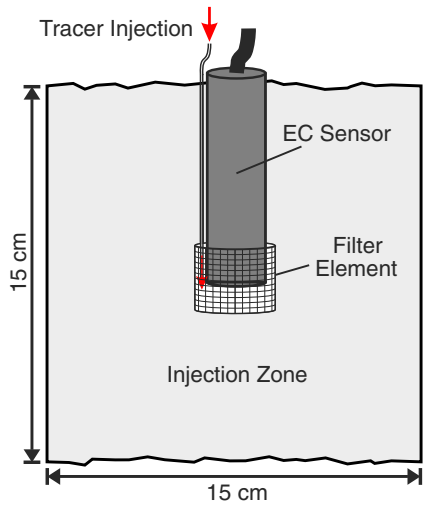

Fig. 2 Vertical cross-section of the experimental configuration within the injection zone

volume of the filter element to enable a meaningful measurement within the filter element. To make sure that the used concentration levels do not provoke density effects which can affect the transport process (Schincariol and Schwartz 1990), a preliminary dye tracer experiment was conducted under similar conditions as the actual tracer experiments—a small amount of dye was added to the 0.3 mol/l potassium chloride solution and injected into the model following the same procedure that was applied in the actual tracer experiments. At the outflow plane, the dye could be visually observed to exit the sediment packing at approximately the same vertical position as it was introduced at the injection zone. This indicates a horizontal tracer movement through the sediment and suggests that under the given experimental conditions, tracer migration appears to be widely unaffected by density effects.

Interpretation of laboratory measured concentrations

Tracer concentrations were measured (1) within the filter element in which tracer was injected, and (2) in the outlet chamber. The aim of these measurements is to quantify, as a function of time, the solute flux entering the porous medium at the injection location (tracer-input function); and the solute flux exiting the porous medium at the outflow plane (BTC).

Monitoring concentrations within the filter element allows one to determine how tracer is transferred from the filter element into the porous medium. Assuming that diffusion is small compared to advection, that the volume within the filter element is well mixed and that the disturbance of the flow rate through the filter element during the injection step is negligible, then concentrations measured within the filter element represent flux concentrations, describing the solute flux from the filter element into the porous medium.

As the fluid exiting the sediment packing is permanently mixed in the outlet chamber, concentrations measured in the outlet chamber can be assumed to be flux averaged. However, the continuous mixing within the chamber produces an increased spreading and a shift on the time axis, of the measured concentration curves. To infer flux averaged BTCs passing the cross-sectional area between sediment packing and outlet chamber from the concentration curves measured in the outlet chamber, the following approach was applied. The mass balance for the tracer contained in the chamber fluid can be formulated as

$$\frac{\partial C}{\partial t} = \frac{Q}{V}(C_{\text{in}} - C_{\text{out}}), \tag{1}$$

in which C is the concentration within the outlet chamber, t is the time, Q is the volumetric flow rate through the chamber, V is the fluid volume within the chamber, C_{in} is the concentration of the fluid entering the chamber, C_{out} is the concentration of the fluid exiting the chamber. Since the experiments were carried out under stationary flow conditions, the flow rate Q and the chamber volume V remained constant during an experiment. Q was determined by collecting the water exiting the model in a reservoir whose weight was measured as a function of time with a balance (accuracy: ± 1 g). V was deduced from head measurements (accuracy: ± 0.2 mm) in the outlet chamber.

For short time intervals Δt, the following approximations can be made:

$$\frac{\partial C}{\partial t} \approx \frac{\Delta C}{\Delta t}, \tag{2}$$

$$C_{\text{out}}(t + \Delta t/2) \approx \frac{C(t) + C(t + \Delta t)}{2}. \tag{3}$$

Substituting Eq. (3) into Eq. (1) and solving for C_{in} yields

$$C_{\text{in}}(t + \Delta t/2) = \left[\frac{C(t + \Delta t) - C(t)}{\Delta t}\right]\frac{V}{Q} + \frac{C(t) + C(t + \Delta t)}{2}. \tag{4}$$

Since V, Q and $C(t)$ were measured during the experiments, Eq. (4) can be used to estimate $C_{\text{in}}(t)$, which represents the flux concentrations passing the cross-sectional area at the end of the sediment packing before being mixed in the outlet chamber. Since the accuracy of Eq. (4) depends on the temporal resolution of the measured data, its applicability was checked using synthetic data—for a synthetic test case, a typical tracer breakthrough (dashed line, Fig. 3) is assumed to describe the solute flux entering the outlet chamber. The resulting concentration curve that would be measured in the permanently mixed outlet chamber can be modeled (solid line) as

$$C(t + \Delta t) = C(t) + \frac{Q\Delta t}{V}[C_{\text{in}}(t + \Delta t) - C_{\text{out}}(t)]. \tag{5}$$

DOI 10.1007/s10040-013-0962-7

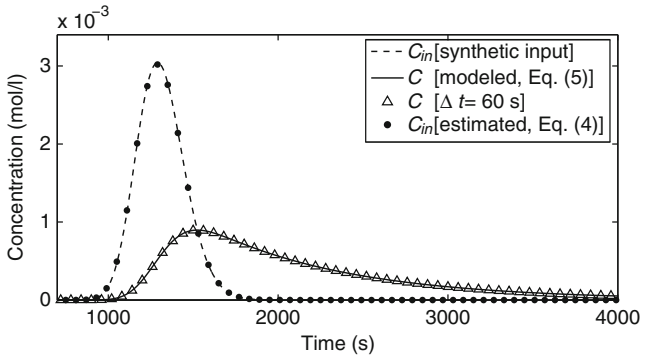

Fig. 3 Synthetic test case to check the functionality of Eq. (4) to estimate flux averaged BTCs (C_{in}) from concentrations measured in the permanently mixed outlet chamber (C)

Note that Eq. (5) applies only for small Δt because it approximates the concentration of the fluid exiting the chamber during a timestep as the chamber concentration calculated for the previous time step.

As is obvious in Fig. 3, the mixing within the outlet chamber produces a strongly smoothened concentration curve in the outlet chamber (solid line) which represents only very poorly the solute flux into the chamber (dashed line). To mimic the temporal resolution of the measurements available from the sandbox experiments, the modeled chamber concentrations are discretized in time with Δt=60 s (triangles). Equation (4) is then applied on the discretized data set. The good agreement between estimated solute flux (dots) and initial synthetic input signal suggests that the temporal resolution, Δt=60 s, of the experimental data is sufficiently high for the application of Eq. (4) to derive flux averaged BTCs from measured chamber concentrations.

Numerical modeling

Numerical simulations analogous to the sandbox experiments were conducted in a numerical model that was parameterized with the properties of the sediments used in the sandbox. Numerical modeling was carried out using the finite elements based Software FEFLOW (Diersch 1996). Flow and transport were computed in a two-dimensional (2-D) depth-averaged model. The domain geometry is illustrated in Fig. 4. Relevant parameters are provided in Table 2. Constant head boundaries were specified at the left and right domain boundaries enforcing flow from left to right. The upper and lower boundaries represent no-flux boundaries for both flow and transport. Initial concentration values are zero in the entire domain. The fluid entering the model (left) has a prescribed concentration of zero. The outflow boundary (right) is unrestricted, allowing tracer to advectively exit the domain. Tracer is introduced via a vertical line source, which is 4 cm long and located in the middle of the injection zone. The length and the position of the line source correspond to the vertical length and location of the filter element in which tracer was injected in the sandbox experiments.

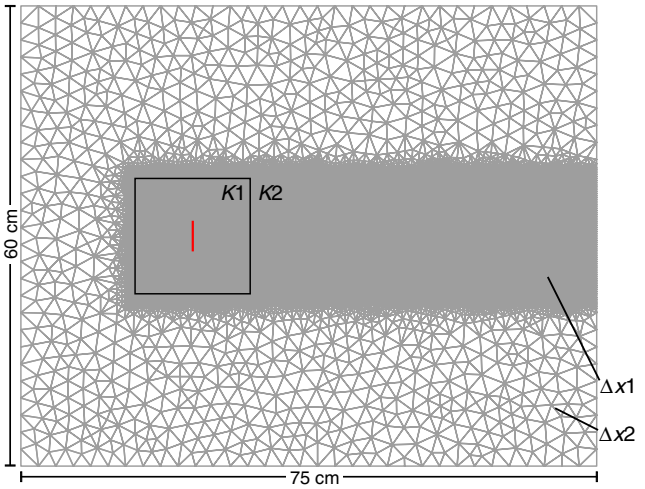

Fig. 4 Numerical model. *K1*, *K2* denote the hydraulic conductivity within the injection zone and surrounding the injection zone, respectively. The *black square* indicates the boundaries of the injection zone (15×15 cm). The *red line* represents the line source. *Δx1*, *Δx2* denote the grid spacing

To simulate the laboratory tracer injection procedure in the numerical model, fixed concentrations, c=0.3 mol/l, and a volumetric fluid flux into the model, Q=4.9 ml/s, were assigned for a step pulse from t_{start}=0 until t_{end}=20 s to the nodes located on the line source. This results in the step pulse injection of a defined fluid volume with a prescribed tracer concentration, evenly distributed over the nodes located on the line source. Q calculates as

$$Q = f\frac{V}{i\Delta t}. \tag{6}$$

V is the volume of tracer solution that was injected in the sandbox (V=50 ml), i is the number of nodes located on the line source (i=17), Δt is the injection duration (Δt=20 s). f is a scaling factor, that is necessary because the numerical model is two-dimensional. The 2-D model represents the vertical projection of a depth-averaged medium with a horizontal thickness of 1 m. The line source, thus, represents an area with dimensions 4 cm× 100 cm, occupying the entire model thickness. Due to this source geometry, the flow field disturbance going along with the injection of a volume of 50 ml tracer solution (as in the sandbox) would be negligible in the numerical model. To come up with a reasonable approximation, f

Table 2 Numerical model parameters

Parameter	Symbol	Unit	Value
Model discretization			
Grid spacing	$\Delta x1$, $\Delta x2$	[m]	0.003, 0.03
Time step	Δt	[s]	0.1
Flow parameters			
Head difference	Δh	[m]	0.023
Hydraulic conductivity	K	[m/s]	see Table 1
Transport parameters			
Porosity	n	[–]	0.45
Local dispersivity	λ_L, λ_T	[m]	0.0022, 0.00022

DOI 10.1007/s10040-013-0962-7

was introduced into Eq. (6) representing the ratio between the horizontal thickness of the numerical domain and the diameter of the filter element used in the sandbox (i.e. f=100 cm/3 cm).

Similar to the laboratory measurements, tracer concentrations in the numerical model were monitored at the source zone and BTCs were recorded at the outflow boundary. For the former, local concentrations were averaged over the nodes located on the line source; for the latter, the summed mass flux through the outflow boundary was divided by the summed fluid flux through that boundary.

To mimic the different sandbox setups in the numerical model, hydraulic conductivity values obtained from Darcy experiments for the different sediments were used to parameterize the hydraulic conductivity in the numerical model (Table 1). The difference in hydraulic head between the inlet and the outlet, Δh, was prescribed according to the head difference that was adjusted in the sandbox experiments. A uniform porosity, n, and uniform dispersivities, λ_L and λ_T, were prescribed for all setups (Table 2). n=0.45 (–) represents the porosity determined for the sediment which was initially used to homogeneously fill the entire laboratory model. Since the porosities of the other sediments that were subsequently inserted into the injection zone only slightly deviated from this value (± 0.02), the porosity in the numerical model was uniformly prescribed as n=0.45 (–) for all setups. The dispersivity values were delineated from the tracer experiment conducted in the homogeneous sandbox (setup hm; see Table 1). The longitudinal dispersivity (λ_L=0.0022 m) represents the value obtained by fitting Eq. (12) to the BTC hm (see Fig. 6b). For the transverse dispersivity, the common approximation λ_T=1/10λ_L (e.g. Delleur 1998) was used.

The numerical domain was discretized in space, $\Delta x1 \approx 0.003$ m, and time, Δt=0.1 s. The level of discretization complies with the Courant and Peclet criteria. Due to the geometry of the line source, a relatively large portion of the numerical domain was not affected by solute migration. To save computational power, a coarser grid size, $\Delta x2 \approx 0.03$ m, was applied to those parts of the numerical domain where no transport occurred (see Fig. 4).

Analytical modeling

Least-squares fits of the 1-D CDE

Conservative transport in a 1-D homogeneous medium during steady flow is generally described using the 1-D CDE:

$$\frac{\partial C}{\partial t} = -v\frac{\partial C}{\partial x} + v\lambda\frac{\partial^2 C}{\partial x^2}, \tag{7}$$

in which C is the fluid concentration, t is time, x is distance and v and λ are the solute velocity and aquifer dispersivity, respectively.

If the tracer is applied instantaneously at t=0, x=0 and concentrations are measured in flux, an analytical solution of Eq. (7) is (Kreft and Zuber 1978):

$$C(x,t) = \frac{M}{Q}\frac{x}{\sqrt{4\pi\lambda v t^3}}\exp\left[-\frac{(x-vt)^2}{4\lambda v t}\right], \tag{8}$$

where M is the amount of tracer injected and Q is the volumetric flow rate.

For a step-type continuous tracer injection and concentration measurement in flux, a solution of Eq. (7) is (Kreft and Zuber 1978):

$$C(x,t) = \frac{C_0}{2}\operatorname{erfc}\left[\frac{x-v(t-t_{on})}{\sqrt{4\lambda v(t-t_{on})}}\right] + \frac{C_0}{2}\exp\left(\frac{vx}{\lambda v}\right)\operatorname{erfc}\left[\frac{x+v(t-t_{on})}{\sqrt{4\lambda v(t-t_{on})}}\right], \tag{9}$$

with C_0 the injection concentration and t_{on} the time when the step injection starts. To simplify the notation, Eq. (9) can be expressed as

$$C(x,t) = f(C_0, x, t_{on}, v, \lambda). \tag{10}$$

Based on superposition, this solution can be extended for a step pulse injection (van Genuchten and Alves 1982):

$$\begin{aligned} C(x,t) &= g(C_0, x, t_{on}, t_{off}, v, \lambda) \\ &= f(C_0, x, t_{on}, v, \lambda) - f(C_0, x, t_{off}, v, \lambda), \end{aligned} \tag{11}$$

where t_{on} is the time when the injection starts and t_{off} is the time when the injection stops. Using again the principle of superposition, Eq. (11) can be extended for a complex tracer-input function consisting of n injection steps (Englert et al. 2007):

$$C(x,t) = \sum_{i=1}^{n} g[C_0(i), x, t_{on}(i), t_{off}(i), v, \lambda], \tag{12}$$

where i is the number of a particular injection step.

Temporal moment analysis

The normalized first temporal moment $\tau_1(x)$ and the normalized second central temporal moment $\tau_{2c}(x)$ of a BTC measured at location x are defined as:

$$\tau_1(x) = \int_0^\infty tc(x,t)dt, \tag{13}$$

$$\tau_{2c}(x) = \int_0^\infty t^2 c(x,t)dt - {\tau_1}^2(x), \tag{14}$$

with $c(x,t)$ the normalized concentration,

$$c(x,t) = \frac{C(x,t)}{\int_0^\infty C(x,t)dt} = \frac{C(x,t)}{\tau_0(x)}, \tag{15}$$

where $C(x,t)$ is the absolute concentration and $\tau_0(x)$ is the BTC's zeroth moment.

 DOI 10.1007/s10040-013-0962-7

If the solute is applied instantaneously at t=0, x=0 and observed concentrations $C(x,t)$ are flux concentrations, then $c(x,t)$ represents a distribution of solute travel times; and the average solute travel time, μ_t, and the variance of solute travel times, σ_t^2, are related to τ_1 and τ_{2c} as

$$\mu_t = \tau_1, \tag{16}$$

$$\sigma_t^2 = \tau_{2c}. \tag{17}$$

Travel time characteristics μ_t and σ_t^2 can be used to calculate transport parameters (Kreft and Zuber 1978):

$$v = \frac{x}{\mu_t}, \tag{18}$$

$$\lambda = \frac{\sigma_t^2 x}{2\mu_t^2}, \tag{19}$$

with the mean flow in the x direction. The definitions for v and λ in Eqs. (18) and (19) are consistent with the relation between transport parameters v and λ of the 1-D CDE and the temporal moments of BTCs predicted by the 1-D CDE.

To account for a tracer-input function different from an instantaneous injection profile, Eqs. (18) and (19) can be modified (Englert et al. 2009):

$$v = \frac{x}{\Delta\mu_t}, \tag{20}$$

$$\lambda = \frac{\Delta\sigma_t^2 x}{2\Delta\mu_t^2}, \tag{21}$$

with

$$\Delta\mu_t = \mu_{t,\mathrm{BTC}} - \mu_{t,\mathrm{input}}, \tag{22}$$

$$\Delta\sigma_t^2 = \sigma_{t,\mathrm{BTC}}^2 - \sigma_{t,\mathrm{input}}^2, \tag{23}$$

where $\mu_{t,\ \mathrm{BTC}}$ and $\sigma_{t,BTC}^2$ represent the average and the variance of a BTC observed at distance x from the injection; $\mu_{t,\ \mathrm{input}}$ and $\sigma_{t,input}^2$ are the average and the variance of the tracer-input function.

Calculation of the average μ_t and the variance σ_t^2 of a distribution from its moments according to Eqs. (13) and (14) is relatively sensitive to measurement errors or data noise. More robust estimates for μ_t and σ_t^2 can be obtained from the percentiles of a distribution, i.e., average and variance can be estimated from the median and the squared absolute value of half the difference between the 15.87 percentile and the 84.13 percentile of the cumulative concentrations. For a normal distribution these percentile based estimates correspond to μ_t and σ_t^2 (e.g. Bulmer 1979).

Results and discussion

Data reliability

Tracer concentrations in the laboratory experiments were deduced from EC measurements. EC values of standard solutions were well reproducible in repeated measurement (deviations of less than 1 %). Calibration curves obtained before and after each experiment showed only negligible drift during the experiments (2 % maximal deviation for a single value). Tracer mass recoveries were calculated for each experiment by dividing the product of the BTC's zeroth temporal moment and the volumetric fluid flux through the model by the injected tracer mass (Table 3). The mean absolute deviation from 100 % amounts to 2.1 % indicating only minor errors in measurement and data processing.

The accuracy of the numerical solution was examined by running the model repeatedly while gradually increasing the temporal and spatial discretization. In particular, convergence of computed BTCs and tracer-input functions was checked for the setups for which the strongest contrasts between the hydraulic conductivity of the source zone and the surrounding material were prescribed: setups LP2 and HP3 (see Table 1). Since these setups showed the largest differences in local flow velocities and the strongest concentration gradients, these setups can be regarded as the most sensitive to numerical dispersion.

General plume behavior

Figure 5 shows snapshots of concentration distributions computed in the numerical model for the setups HM, HP3 and LP2, corresponding to a homogeneous setup, a high-permeable injection zone setup and a low-permeable injection zone setup, respectively (see Table 1). Obviously, the different hydraulic setups lead to distinctly different plume characteristics. While the plume resulting from tracer injection into the high-permeable injection zone is characterized by a larger transverse and a smaller longitudinal spreading compared to the plume evolving in the homogeneous medium, the plume originating from a low-permeable injection zone is characterized by a smaller transverse and a stronger longitudinal spreading compared

Table 3 Tracer mass recovery

Laboratory experiment	Mass recovery [%]
lp2	103.2
lp1	100.2
hm	98.7
hp1	95.5
hp2	101.1

DOI 10.1007/s10040-013-0962-7

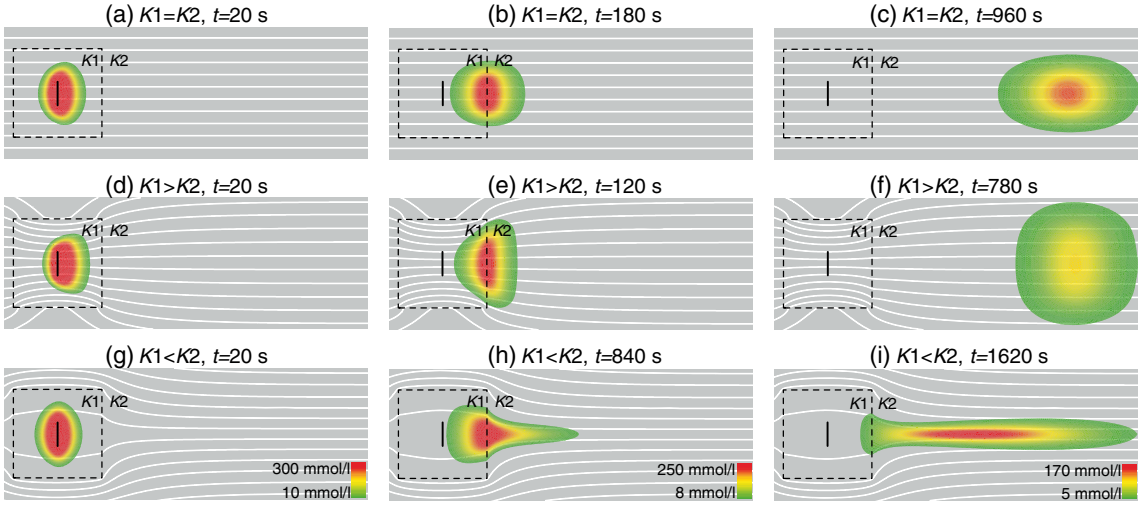

Fig. 5 Streamlines and plume development computed in the numerical model. **a-c** Homogeneous setup HM, **d-f** high-permeable injection zone setup HP3, **g-i** low-permeable injection zone setup LP2. Shown are snapshots of spatial concentrations at different times: at the end of tracer injection (*left*), when the plume's center exits the injection zone (*middle*), when first concentrations arrive at the detection plane (*right*)

to the homogeneous setup. This is a consequence of the different flow field characteristics at the source zone. In the case of a high-permeable injection zone, streamlines (indicated in white color in Fig. 5) converge before entering the source zone, i.e., the volumetric fluid flux through the source zone is relatively large. As a result, tracer is "flushed" out of the injection zone relatively fast. After passing the source zone, streamlines diverge, which enlarges the plume's transverse spreading. The tracer plume reaches the detection plane slightly earlier compared to the homogeneous setup. The opposite occurs when tracer is injected into a low-permeable injection zone. Streamlines diverge upstream of the source zone, which leads to a relatively small volumetric fluid flux through the source zone. As a result, tracer remains within the injection zone for a relatively long time. After having passed the injection zone boundary, tracer is transported downstream much faster than tracer that is still trapped within the injection zone. This strongly increases the longitudinal spreading of the plume, while streamline convergence downstream of the source zone reduces the transverse plume spreading. The tracer plume arrives at the detection plane distinctly later compared to the homogeneous setup.

Note that the source zone hydraulic conditions determine the volume of the medium which is sampled by the plume on its way from the source to the detection plane. The sampled volume depends on the plume's width which is larger for the high-permeable injection zone setup and smaller for the low-permeable injection zone setup compared to the homogeneous setup.

Tracer-input functions and BTCs

Figure 6a,c presents measured and modeled tracer-input functions for the different hydraulic setups. In the laboratory model, tracer-input functions were measured within the filter element in which tracer was injected; in the numerical model, tracer-input functions were recorded on the nodes located on the line source.

When the tracer injection begins (at $t=0$) the laboratory concentrations increase rapidly until they nearly reach the concentration level of the injected tracer solution. When the tracer injection ends (at $t=20$ s), concentrations stay roughly constant for some time and then decrease slowly with time. The lower the hydraulic conductivity of the injection zone, the slower the decrease of concentrations. This is due to different volumetric flow rates through the source zone induced by the different hydraulic setups. The volumetric flow rate through the source zone is controlled by the injection zone's hydraulic conductivity relative to the surrounding hydraulic conductivity. If the injection zone's hydraulic conductivity is high, tracer is quickly flushed out of the filter element and thus released into the porous medium relatively fast. If the injection zone's hydraulic conductivity is low, tracer remains for a relatively long time within the filter element. This results in a slow tracer release from the filter element into the porous medium.

It is important to note that the measured tracer-input functions, especially those measured in low-permeable injection zones, deviate distinctly from the function describing the injection of tracer from the syringe into the filter element. The latter was the same for all experiments and is indicated by the black colored step profile in Fig. 6a. This clearly demonstrates the necessity to monitor concentration at the location where tracer is injected to derive adequate tracer-input functions.

Figure 7a, b depicts the temporal moments of tracer-input functions which were calculated using Eqs. (13) and (14). The first and second moments of laboratory tracer-input functions generally increase with decreasing permeability of the injection zone because relatively wide tracer-input functions were obtained for low-permeable injection zone setups and relatively short tracer-input functions were obtained for high-permeable injection zone setups. The only

 DOI 10.1007/s10040-013-0962-7

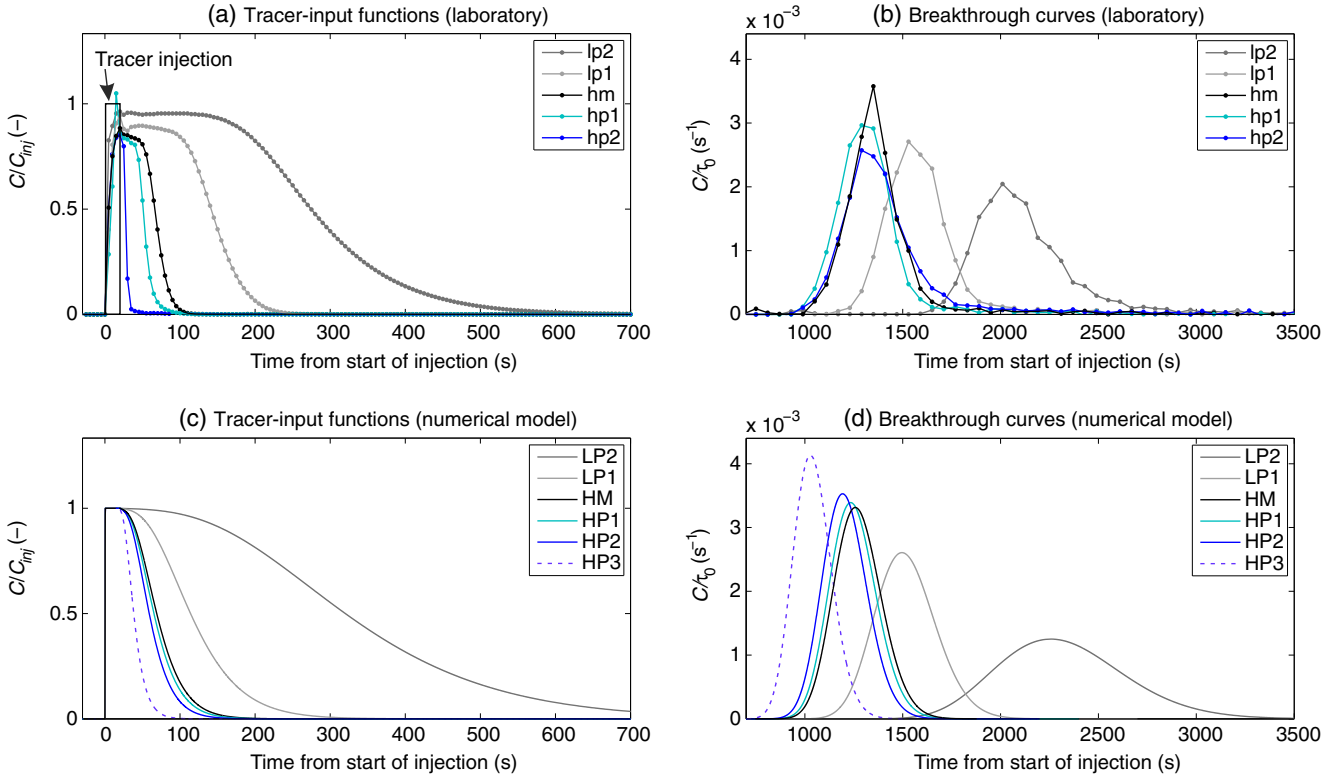

Fig. 6 Tracer-input functions and BTCs for the different hydraulic setups (see Table 1). **a** Laboratory tracer-input functions measured at the location where tracer was injected, **b** laboratory BTCs obtained after applying Eq. (4) to the concentrations measured in the outlet chamber, **c** tracer-input functions recorded on the nodes located on the line source in the numerical model, **d** summed mass flux divided by the summed fluid flux through the outflow boundary in the numerical model. Tracer-input functions are normalized by the concentration of the injected tracer solution; BTCs are normalized by their zeroth temporal moment

exemption is τ_{2c} of the laboratory tracer-input function hp2, which is slightly larger than τ_{2c} of the tracer-input function hp1. This is due to slow concentration decrease at very low concentration levels in the tracer-input function hp2, which is hardly visible in Fig. 6a but enlarges τ_{2c}.

Figure 6c presents tracer-input functions computed in the numerical model. Generally, the modeled concentrations reflect relatively well the laboratory measurements in the sense that the overall shape of the laboratory tracer-input functions is reproduced and the rate of decrease of modeled concentrations depends on the hydraulic conductivity of the injection zone in a rather similar manner as observed in the laboratory model. This suggests that the representation of the injection procedure in the numerical simulations captures relatively well the tracer injection procedure in the laboratory

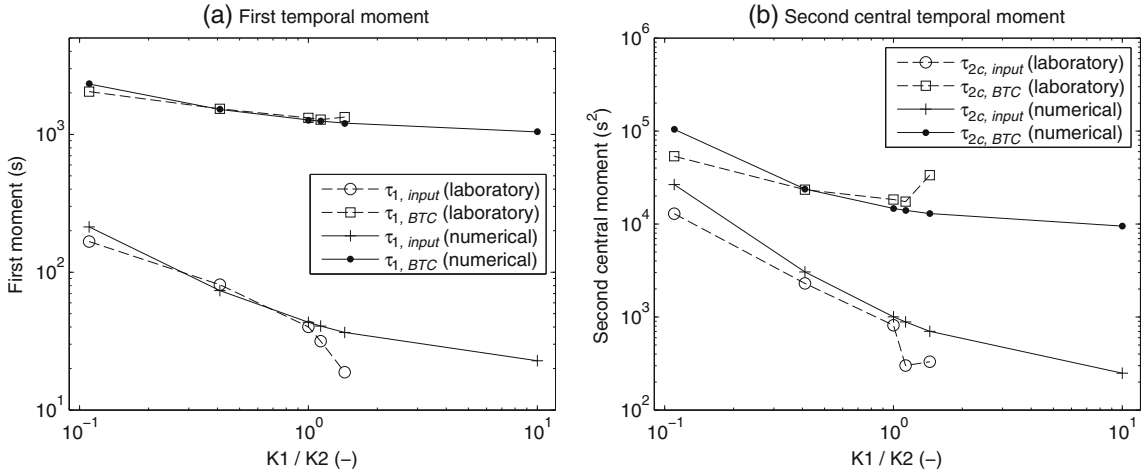

Fig. 7 Temporal moments of tracer-input functions and BTCs. The *x*-axis denotes the ratio between the hydraulic conductivity of the injection zone and the surrounding material (see Table 1). **a** $\tau_{1,\ input}$ and $\tau_{1,\ BTC}$ refer to the first temporal moment of the tracer-input function and the tracer BTC, respectively. **b** $\tau_{2c,\ input}$ and $\tau_{2c,\ BTC}$ refer to the second central temporal moment of the tracer-input function and the tracer BTC, respectively

 DOI 10.1007/s10040-013-0962-7

experiments. As described in a previous section Numerical modeling, a fluid flux boundary condition was prescribed in the numerical simulations for the line source during the injection step. This boundary condition is supposed to simulate the disturbance of the flow field due to the injection of tracer solution. The fluid flux boundary condition turned out to be essential to reproduce the tracer-input functions measured in the laboratory model. The fluid injection provokes a disturbance of the flow field at the source zone, which causes tracer to be initially spread in all directions around the line source (see Fig. 5). When discharge through the injection zone establishes again after the injection procedure, some amount of tracer migrates back into the source zone. This induces the plateau-like behavior and the gradual concentration decrease apparent in the tracer-input functions. Though not presented in Figs. 5 and 6, note that if the flow field disturbance during injection is not accounted for in the numerical model by prescribing a fluid flux boundary for the duration of the tracer injection step, the initial concentration distribution at the end of the tracer injection is considerably less spread, concentrations decrease much faster at the source zone and the laboratory tracer-input functions are not well reproduced. This clearly points out the importance of considering the hydraulic effects of the tracer injection process in laboratory or field experiments in order to realistically model tracer injection in numerical simulations.

However, comparing in detail measured and modeled tracer-input functions, it appears that the laboratory tracer-input functions generally decrease slightly faster than the numerically modeled concentrations. As a consequence, the laboratory tracer-input functions are less spread which leads to smaller second temporal moments compared to the numerical results (see Fig. 7b). As shall be discussed now, possible explanations for these deviations between laboratory measured and numerically modeled tracer-input functions might be flow focusing and mixing induced by the filter element in which tracer was injected in the laboratory experiments. Further differences between laboratory and modeling results might result from the reduction of the transport process to a 2-D problem in the numerical simulations.

The filter element in which tracer was injected in the laboratory experiments represents a high-permeability inclusion within the sediment packing, because its hydraulic conductivity is larger than the hydraulic conductivity of the surrounding sediment. This locally focuses the flow field and leads to a larger volumetric flow rate through the cross-section of the filter element compared to the flow rate through an equivalent cross-section within the porous medium. Since this effect is not accounted for in the numerical model, it can be expected that the flow rate through the filter element in the laboratory experiments was larger than the flow rate through the source zone computed in the numerical model, which may explain the faster decrease of concentration in the laboratory tracer-input functions compared to the numerical results.

The filter element's inner volume excluding the portion which is filled by the EC sensor amounts to approximately 15 ml. This volume represents a mixing volume which is not considered in the numerical model and thus, might lead to differences between measured and modeled concentrations. If the volume within the filter element was permanently well mixed, this would slow down the decrease of concentration subsequent to tracer injection. However, the filter element did not contain a mixing device so that complete mixing within the filter element is not necessarily fulfilled. Moreover, the mixing volume (15 ml) is only small compared to the volume of the injected tracer solution (50 ml), so that the effects of mixing can be expected to be only small.

Since the volume of the injected tracer solution exceeds the volume of the filter element, tracer is spread in all directions around the filter element during the injection. Due to the two-dimensionality of the numerical model, the tracer spreading during the injection in the numerical simulations is limited to two dimensions only. This may lead to a larger initial plume spreading in the numerical simulations compared to the laboratory experiments, and thus, to wider tracer-input functions obtained in the numerical model.

Tracer breakthrough at the downgradient detection plane is depicted in Fig. 6b, d. Laboratory BTCs were derived by applying Eq. (4) on the concentration curves measured in the outlet chamber; numerical BTCs were calculated by dividing the summed mass flux through the outflow boundary by the summed fluid flux through that boundary. Temporal moments of BTCs are presented in Fig. 7a, b. Moments of laboratory BTCs represent robust percentile-based estimates (see section Analytical modeling) because moments calculated with Eqs. (13) and (14) were found to be tremendously distorted by data noise. For the numerical BTCs, percentile-based moment estimates deviate less than 1 % from moments calculated using Eqs. (13) and (14).

The results clearly show that different hydraulic injection zone setups lead to considerably different BTC characteristics. In particular, the mean arrival time and spreading of BTCs and the peak concentration levels at the detection plane are strongly affected by the hydraulic conditions at the injection zone. While low-permeable injection zone setups lead to relatively wide BTCs that are characterized by late mean arrival times and low peak concentrations, high-permeable injection zone setups produce relatively steep BTCs with high peak concentrations and early mean arrival times. Accordingly, the first and second temporal moments of BTCs generally increase with decreasing hydraulic conductivity of the injection zone. Results from laboratory experiments and numerical simulations agree fairly well regarding the general trend, however, notable differences exist for individual BTCs. Most distinct are the deviations between laboratory and numerical results for the setups in which the injection zone has the highest hydraulic conductivity and the lowest hydraulic conductivity, respectively: The laboratory BTC lp2 is characterized by a smaller first and second moment compared to the numerical equivalent LP2 (see temporal

 DOI 10.1007/s10040-013-0962-7

moment values at $K1/K2=0.11$ in Fig. 7). The laboratory BTC hp2, on the other hand, is characterized by a larger first and second moment compared to the numerical BTC HP2 (see temporal moment values at $K1/K2=1.44$ in Fig. 7). Partly, this can be explained with the differences between measured and modeled tracer-input functions, i.e., the smaller first and second temporal moments of the laboratory tracer-input function lp2 compared to the numerical tracer-input function LP2 naturally lead to smaller first and second temporal moments of the laboratory BTC lp2 compared to the numerical BTC LP2. However, this cannot explain the larger moments of the laboratory BTC hp2 compared to the numerical BTC HP2, because in this case, the moments of the laboratory tracer-input function hp2 are actually smaller than the moments of the numerical tracer-input function HP2. These deviations might be the result of small-scale heterogeneous structures within the sediment packing which induce a different dispersion behavior in the laboratory model and in the numerical model. In the numerical simulations, parameters are, except for the hydraulic conductivity contrast between the injection zone and the surrounding medium, homogeneously distributed throughout the entire domain. In the laboratory model, however, the sediment packing is not perfectly homogeneous. Even the highly uniform sand used for the homogeneous packing shows some variability in grain size, which gives rise to small-scale heterogeneous structures in the sand-packing. The occurrence of non-homogeneous structures in apparently homogeneously packed columns and their effect on transport processes have already been reported in several other studies (e.g. Huang et al. 1995; Levy and Berkowitz 2003; Cortis and Berkowitz 2004). In heterogeneous media, the dispersivity scales with the observation volume. As is obvious in Fig. 5, the volume sampled by the tracer plume is mainly controlled by the transverse plume spreading, which, in turn, depends on the hydraulic conditions at the source zone. The plume resulting from tracer injection into a high-permeable injection zone is stretched in the transverse direction, and thus, samples a larger volume on its way to the detection plane compared to the homogeneous setup. In contrast, the transversally narrow plume resulting from injection into a low-permeable injection zone samples a smaller volume than the plume in the homogeneous setup. If the sediment packing is heterogeneous, this will lead to an enlarged dispersion for the high-permeable injection zone setups and a decreased dispersion for the low-permeable injection-zone setups in the laboratory experiments. In the numerical model this effect does not occur because the material surrounding the injection zone is perfectly homogeneous and dispersion is, thus, not scale-dependent. Since the dispersivity in the numerical model was prescribed according to the apparent dispersivity derived from the homogeneous laboratory tracer experiment, this could explain the smaller spreading of the laboratory BTC lp2 and the larger spreading of the laboratory BTC hp2 compared to their numerical equivalents.

Transport characterization

Breakthrough curve analyses were performed to derive advective–dispersive transport parameters (see section Analytical modeling). Such analyses interpret the BTCs as if they were measured in a fictitious uniform medium. The sediments in the sandbox model are, however, not homogeneous, i.e., description of transport with the 1-D CDE becomes a simplified model. The obtained transport parameters, thus, represent apparent transport parameters, v_a and λ_a, which are based on a simplified, 1-D interpretation of the transport process.

Tracer-input functions measured at the location where tracer was injected were explicitly considered in the analysis of BTCs by applying the following two approaches. In the first approach, apparent transport parameters were derived by fitting Eq. (12) to the BTCs. Thereto, the measured tracer-input functions were discretized in time and separated into n injection steps (see e.g. Fig. 8b), each of which is considered as a boundary condition for an analytical solution of the 1-D CDE in Eq. (12). The second approach is based on temporal moments and calculates apparent transport parameters from the changes of the first and second temporal moment along the distance between injection and detection. Thereto, temporal moments of BTCs and measured tracer-input functions were calculated, after which Eqs. (20)–(23) were applied to derive apparent transport parameters.

To investigate which effects on apparent transport parameters result from the use of simplified tracer-input approximations, apparent transport parameters were also derived based on the assumption of an instantaneous tracer input (Dirac pulse at $t=0$) and a step pulse tracer-input profile ($t_{on}=0$, $t_{off}=20$ s), respectively. The 20-s step pulse corresponds to the duration over which tracer was injected in the experiments. Based on the Dirac pulse tracer-input approximation, apparent transport parameters were obtained by fitting Eq. (8) to the BTCs; and by applying Eqs. (20) and (21) with $\Delta\mu_t=\mu_{t,\ BTC}$ and $\Delta\sigma_t^2=\sigma_{t,BTC}^2$. Based on the step pulse tracer-input approximation, apparent transport parameters were obtained by fitting Eq. (11) to the BTCs; and by applying Eqs. (20) and (21) with $\Delta\mu_t=\mu_{t,\ BTC}-\mu_{t,\ step}$ and $\Delta\sigma_t^2=\sigma_{t,BTC}^2-\sigma_{t,step}^2$.

Least-squares fits of the 1-D CDE

Figures 8c and 9c show BTCs and least-squares fits of the 1-D CDE for the sandbox experiment lp2 and the numerical simulation LP2, respectively. While the numerical BTC is perfectly represented by the 1-D CDE, the 1-D CDE fails to capture the early and late time evolution of the laboratory BTC. Similar deviations between measured concentrations and 1-D CDE were obtained for every laboratory experiment, i.e., also for the homogeneous setup. This suggests that some inhomogeneities exist even in the homogeneous sediment packing, leading to a slightly anomalous transport behavior which is not

 DOI 10.1007/s10040-013-0962-7

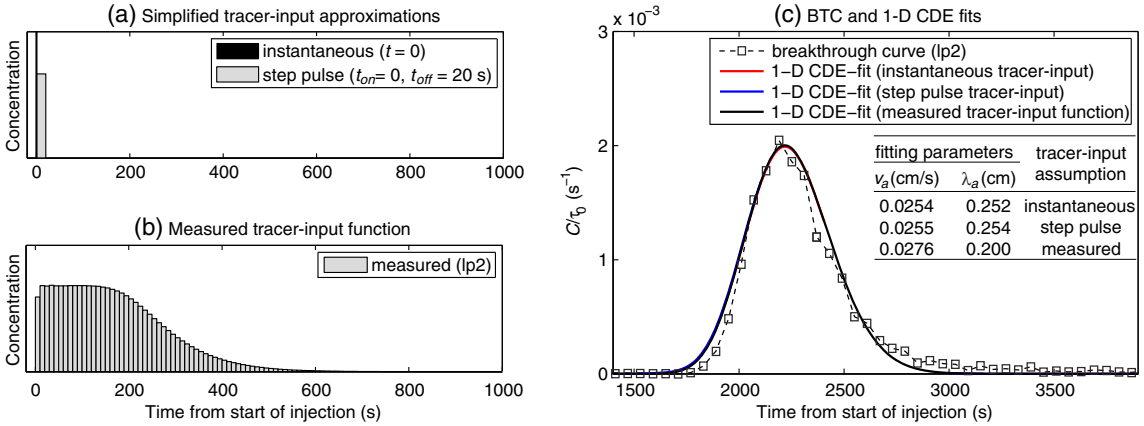

Fig. 8 Least-squares fits of the 1-D CDE for the laboratory experiment lp2. **a**–**b** Tracer-input assumptions, **c** BTC and 1-D CDE fits. Note that the different fit-curves are practically identical and overlay each other in the graph (i.e. the fit-curves *colored in red and blue* are overlain by the *black colored* fit-curve)

described by the 1-D CDE. Note that the deviations between BTC and 1-D CDE are not the result of the hydraulic contrast between injection zone and surrounding material, because then similar deviations between BTC and 1-D CDE should have been obtained in the numerical simulations. All numerical BTCs are, however, perfectly covered by the 1-D CDE.

What is surprising in Figs. 8c and 9c is that the three 1-D CDE fit-curves, although based on different tracer-input assumptions, are practically identical and overlay each other. Explicitly, the three fit-curves are based on the assumption of the tracer-input function being a Dirac pulse, a 20-s step pulse and the measured tracer-input function, respectively. The different tracer-input assumptions are depicted in Figs. 8a, b and 9a, b. Remarkably, the three approaches provide similarly good fits to the BTCs; however, the transport parameters derived by the different approaches are not similar. The individual pairs of fitting parameters corresponding to the three fit-curves are also provided in Figs. 8c and 9c. Compared to the parameters derived by fully accounting for the measured tracer-input functions, the fit-curves that were derived, assuming an instantaneous and a step-pulse tracer-input profile, yield smaller values for the apparent velocity and larger values for the apparent dispersivity. Since the Dirac pulse and the step pulse only poorly represent the actually measured tracer-input function, it can be expected that the so-derived transport parameters are biased. However, the goodness-of-fit gives absolutely no indication as to which set of fitting parameters yields the most appropriate transport parameters. This suggests that the 1-D CDE is capable of adapting rather well to BTCs even if strongly simplified tracer-input functions are assumed and that, despite good agreement between a BTC and a least-squares fit of the 1-D CDE, transport parameters derived as fitting parameters can still be biased if they rely on inadequate tracer-input approximations.

In the laboratory experiment lp2, the approach assuming an instantaneous tracer input underestimates the apparent velocity by 8 % and overestimates the apparent dispersivity by 26 %, compared to the values that were derived by fully accounting for the measured tracer-input function. In the numerical experiment LP2, the apparent velocity is underestimated by 9 % and the apparent dispersivity is overestimated by 11 %. It can be argued that these deviations are not major. However, there is no

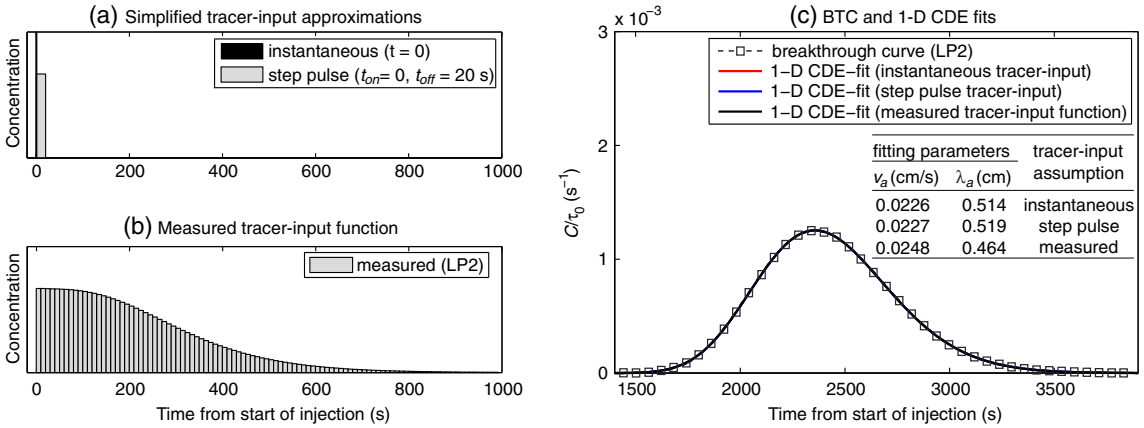

Fig. 9 Least-squares fits of the 1-D CDE for the numerical simulation LP2. **a**–**b** Tracer-input assumptions, **c** BTC and 1-D CDE fits. Note that the different fit-curves are practically identical and overlay each other in the graph (i.e. the fit-curves *colored in red and blue* are overlain by the *black-colored* fit-curve)

 DOI 10.1007/s10040-013-0962-7

indication that for larger discrepancies between assumed and actual tracer-input function, the 1-D CDE would not still be capable of adapting well to a BTC. In that case, significantly stronger deviations between fitting parameters and 'true' transport parameters must be expected. This demonstrates the necessity of monitoring the tracer injection in tracer experiments to obtain adequate tracer-input functions for the analysis of BTCs.

Apparent transport parameters

Figure 10a shows apparent velocities derived from BTCs as a function of the hydraulic contrast between injection zone and surrounding material. Relatively small apparent velocities were obtained when tracer was injected into a relatively low-permeable injection zone; larger apparent velocities were obtained when tracer was injected into a relatively high-permeable injection zone. Since the apparent velocity derived from a BTC represents a path-averaged velocity, integrated over the distance between injection and detection, this trend reflects the different local velocities within the injection zone for the different setups, i.e., relatively small local velocities in low-permeable injection zones and larger local velocities in high-permeable injection zones.

Apparent dispersivities are plotted in Fig. 10b. Here, there is no clear correlation between apparent dispersivities and the permeability of the injection zone. The numerical BTCs yield the largest dispersivities for the low-permeable injection zone setups; the laboratory BTCs yield the largest dispersivities for the high-permeable injection zone setups. As already discussed in the previous section Tracer-input functions and BTCs, this might be the consequence of small-scale inhomogeneities in the sediment packing which cause the dispersivity in the laboratory model to scale with the observation volume. If the dispersivity in the laboratory model is scale-dependent, this will lead to an enlarged dispersion when tracer is injected into a high-permeable injection zone (because the resulting plume samples a relatively large volume of the sediment packing) and a decreased dispersion when tracer is injected into a low-permeable injection zone (because the plume samples a relatively small volume of the sediment packing). Since in the numerical model the dispersivity is not scale-dependent, this might produce, for the high-permeable injection zone setups, larger apparent dispersivities obtained in the sandbox experiments compared to the values derived in the numerical simulations; and for the low-permeable injection zone setups, smaller dispersivities obtained in the sandbox experiments compared to the numerically derived values.

Apparent transport parameters derived from least-squares fits of the 1-D CDE and apparent transport parameters derived from temporal moment analyses are practically identical for the numerical BTCs. For the BTCs measured in the laboratory, the two methods yield different parameters, namely, slightly larger apparent velocities, and distinctly larger apparent dispersivities were calculated by the method of moments compared to the values obtained from 1-D CDE-fits. The reason for this is that the numerical BTCs are almost perfectly captured by the 1-D CDE fits, while the laboratory BTCs are, in contrast, not completely captured by the 1-D CDE fits. Perfect agreement between fit-curve and BTC means that the temporal moments of fit-curve and BTC are identical. In this case, the method of moments and least-squares fits yield similar results. If BTC and fit-curve deviate from each other, the moments of BTC and fit-curve are different which leads to differences in the apparent transport parameters derived by the two methods.

Implications of simplified tracer-input approximations in the analysis of BTCs

Figure 10c–f shows the apparent transport parameters that were derived from BTCs by approximating the tracer-input function as a Dirac pulse (at t=0) or a step pulse (t_{on}=0, t_{off}=20 s), respectively. To focus on the effect of tracer-input assumptions on transport parameters rather than on the absolute transport parameter values, transport parameters are presented as deviations from the parameters that were obtained by fully accounting for the measured tracer-input functions. For the sake of clarity, the values derived from 1-D CDE fits are depicted in Fig. 10c, d and those calculated from temporal moments are depicted in Fig. 10e, f.

Approximating the tracer-input function as a Dirac pulse or a step pulse obviously yields underestimated values for v_a, which plot as negative values in Fig. 10c,e. The lower the permeability of the injection zone is, the stronger the underestimation of v_a. Accordingly, the strongest underestimation of v_a, was obtained for the laboratory setup lp2 (−8 %) and the numerical setup LP2 (−9 %). This can be explained as follows. By approximating the tracer-input function as a Dirac pulse (at t=0) or a step pulse (t_{on}=0, t_{off}=20 s), it is assumed that the entire tracer mass has entered the porous medium at t= 0 (Dirac pulse) or t=20 s (step pulse), respectively. The tracer-input functions that were actually measured, however, show that tracer still entered the porous medium at significantly later times. For example, in the case of the low-permeable injection zone setup lp2, relevant tracer concentrations were found to be released from the source zone until $t\approx$500 s (see Fig. 6a). As a consequence, by approximating the tracer-input function as a Dirac pulse or a step pulse, the tracer's apparent velocity is underestimated, because tracer that enters the porous medium at t>20 s must move faster to reach the detection plane at a given time than tracer which is assumed to enter the porous medium at $t\leq$20 s.

The underestimation of the apparent velocity is more pronounced for the low-permeable injection zone setups because the tracer-input functions that were measured within low-permeable injection zones deviate stronger from the Dirac pulse and the step pulse approximations than those tracer-input functions measured within high-permeable injection zones.

 DOI 10.1007/s10040-013-0962-7

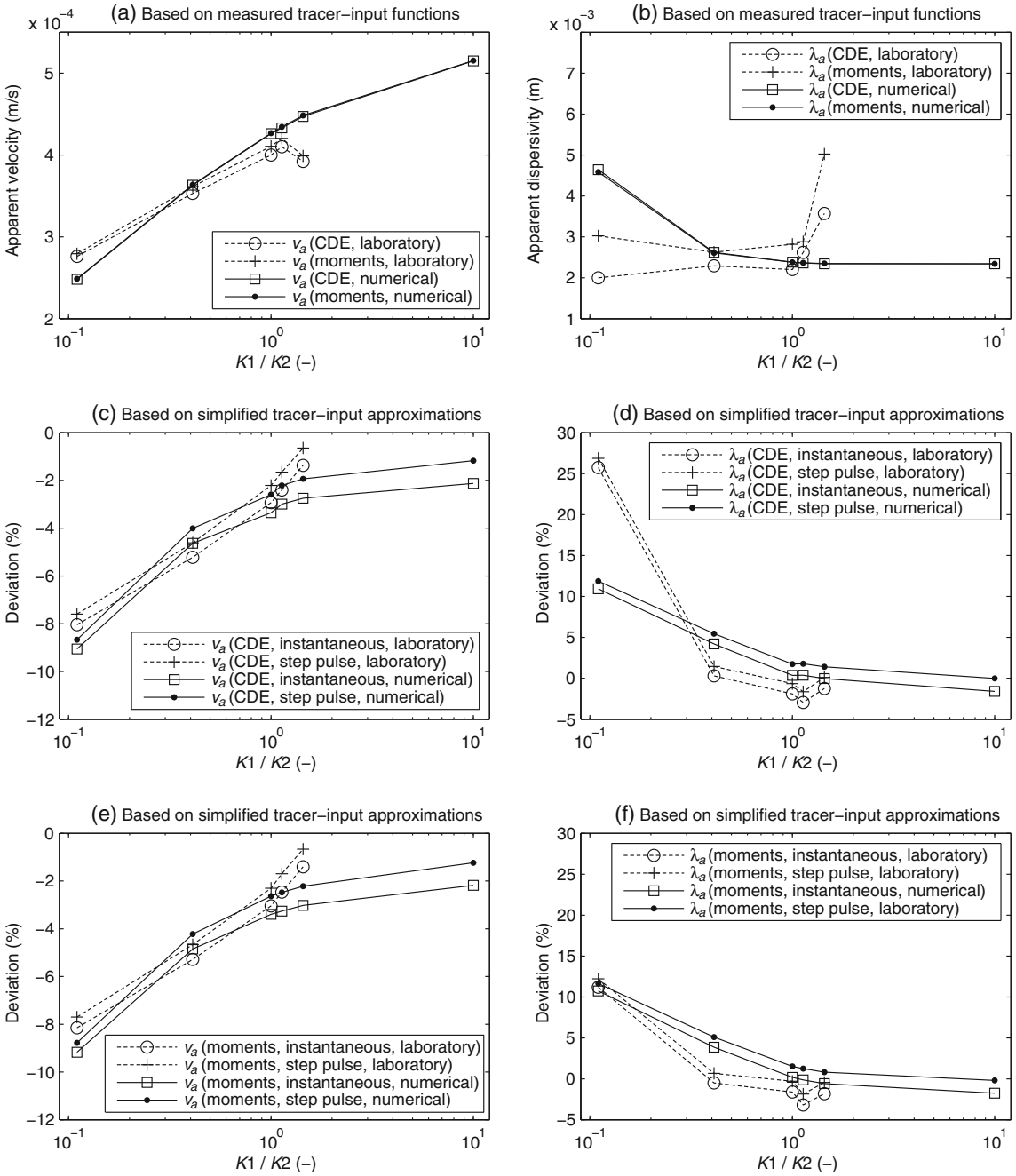

Fig. 10 Apparent transport parameters derived from BTCs using least-squares fits of the 1-D CDE and temporal moment analyses. The *x*-axis denotes the ratio between the hydraulic conductivity of the injection zone and the surrounding material (see Table 1). **a–b** Apparent transport parameters obtained by fully accounting for the measured tracer-input function, **c-f** transport parameters obtained by approximating the tracer-input function as a Dirac pulse and a step pulse (presented values represent deviations from those parameters that were obtained by fully accounting for the measured tracer-input functions)

Note that the differences between apparent transport parameters that were derived assuming a Dirac pulse input and those values which were derived assuming a step pulse input are only small. This is because the BTCs measured in the experiments arrived at the detection plane at relatively late times (i.e. t>1,000 s). For the interpretation of these BTCs, the difference between a Dirac pulse at t=0 or a step pulse from t_{on}=0 until t_{off}=20 s are only minor.

Apparent dispersivities, λ_a, are generally overestimated by approximating the tracer-input function as a Dirac pulse or a step pulse, i.e. they plot as positive values in Fig. 10d, f. The strongest overestimation of λ_a is obtained for the low-permeable injection zone setups lp2 (+26 %, 1-D CDE-fit; +11 %, temporal moments) and LP2 (+11 %, 1-D CDE-fits; +11 %, temporal moments). The reason for this is that when the tracer-input function is approximated as a Dirac pulse (at t=0) or a step pulse (t_{on}=0, t_{off}=20 s), the spreading of the tracer-input function is assumed to be zero in the case of the Dirac pulse and rather small in the case of the step pulse. The spreading of the actually

 DOI 10.1007/s10040-013-0962-7

measured tracer-input functions is considerably larger (see Fig. 6a). As a result, approximating the tracer-input function as a Dirac pulse or a step pulse overestimates the spreading of the BTC due to dispersion. More precisely, it is neglected that the tracer-input function already contributes a spreading which is not the result of dispersion as it is already present when the tracer enters the porous medium. This leads to an overestimation of λ_a. However, as already discussed, by assuming a Dirac pulse or a step pulse tracer input, the apparent velocity gets underestimated, which, interestingly, leads to an underestimation of λ_a. This can be deduced from Eq. (21). If the measured tracer-input function is neglected and tracer is assumed to instantaneously enter the porous medium, then $\Delta\sigma_t^2$ in Eq. (21) gets overestimated, because $\sigma^2_{t,input}$ in Eq. (23) is assumed to be zero. At the same time, $\Delta\mu_t$ in Eq. (21) also gets overestimated, because $\mu_{t,\ input}$ in Eq. (22) is assumed to be zero. While the overestimation of $\Delta\sigma_t^2$ enlarges the estimated value for λ_a, the overestimation of $\Delta\mu_t$ reduces the estimated λ_a. λ_a, thus, depends on the ratio of the overestimation of $\Delta\sigma_t^2$ and the overestimation of $\Delta\mu_t^2$. That is why, for some setups, λ_a gets underestimated by assuming a Dirac pulse or a step pulse tracer input (negative values in Fig. 10d, f), which also explains why the overestimation of λ_a is not as pronounced as might be expected. For example, in the case of the laboratory experiment lp2, neglecting the temporal moments of the measured tracer-input function by assuming an instantaneous input profile leads to an overestimation of $\Delta\sigma_t^2$ in Eq. (21) by 32 %. However, the apparent dispersivity gets overestimated by only 11 % because $\Delta\mu_t$ in Eq. (21) is overestimated by 8 %.

These findings demonstrate that the use of simplified approximations for the tracer-input function can lead to biased transport parameters derived from BTCs. Interpretation of BTCs based on the assumptions of the tracer-input function being a Dirac pulse or a step pulse yielded underestimated values for the apparent velocity and overestimated or underestimated values for the apparent dispersivity, compared to those values derived by explicitly accounting for the measured tracer-input function in the BTC analysis. In the present experiments, the use of simplified tracer-input approximations resulted in only relatively mildly biased v_a and λ_a. This suggests that using simplified approximations for the tracer-input function might yield sufficiently accurate estimates for the apparent transport parameters in many applications. However, the obtained bias of maximally +8 % for v_a and +26 % for λ_a is not negligibly small. Furthermore, it must be noted that different experimental conditions (e.g. larger mixing volume within the injection well, smaller flow rate passing the injection well, multi-peaked tracer injection) might lead to a much stronger disagreement between idealized tracer-input profiles and actual tracer-input function. In such cases, using simplified tracer-input approximations will lead to stronger biased transport parameters. The results therefore suggest that monitoring of the tracer-input function and subsequent consideration of the measured tracer-input function in the analysis of BTCs can improve the estimation of apparent transport parameters from tracer experiments.

Conclusions

The results of the study demonstrate that the hydraulic conditions at the source of a solute are of major importance for plume development. Tracer injection into high-permeability zones causes early arrival, and enhanced transverse and reduced longitudinal spreading. Tracer injection into low-permeability zones causes late arrival, and reduced transverse and enhanced longitudinal spreading. The results therefore suggest that the hydraulic conditions at the source zone are of particular interest for predicting when and at what concentrations a solute reaches a downgradient location, which is a classical goal of risk assessment at contaminated sites. The study therewith supports the findings of Nowak et al. (2010) who investigated optimal sampling strategies and found that characterization of the hydraulic conditions at the source of a contaminant greatly reduces the uncertainty in predicted concentrations.

An interesting aspect of the results is that the hydraulic conditions at the source zone determine the lateral width of a plume and thus, the volume sampled by the plume during its further transport. This is of particular importance for plume dispersion in heterogeneous media because in heterogeneous media, dispersion scales with the observation volume. In the present study, this appears to provoke deviations between laboratory BTCs measured in a slightly heterogeneous sandbox packing and modeled BTCs computed in a homogeneous numerical model.

Apparent transport parameters derived from BTCs were found to change distinctly as a function of the hydraulic conditions at the source zone. This indicates that transport parameters obtained in tracer experiments can be biased towards the hydraulic situation close to the injection well instead of yielding representative aquifer properties.

In the experiments conducted, different source zone hydraulic conditions were arranged by placing a cube-shaped heterogeneous inclusion within an otherwise homogeneous medium. This simple setup was chosen to examine, under well-defined conditions, the effects of source zone hydraulic conditions on plume behavior and BTCs. In real world aquifers, however, the conductivity field is heterogeneous in the entire aquifer, not only in the region close to the source zone. Therefore, additionally to the influence of the hydraulic conditions at the source zone, plume behavior is affected by aquifer heterogeneity farther downstream. Further research is needed to unravel these two effects and to evaluate their contributions to transport characteristics such as plume spreading and BTC properties.

Tracer-input functions measured at the location where tracer was injected were found to deviate distinctly for different hydraulic injection zone setups, although the

 DOI 10.1007/s10040-013-0962-7

tracer injection procedure was the same for all setups. This points out the necessity to monitor concentrations at the injection location in tracer experiments, in order to obtain adequate tracer-input functions.

Tracer-input functions measured in low-permeable injection zone setups were found to depart strongly from idealized approximations such as instantaneous or step pulse tracer-input profiles. It could be demonstrated that the use of simplified approximations for the tracer-input function can lead to biased transport parameters derived from BTCs. By approximating the tracer-input function as a Dirac pulse or a step pulse, underestimated values for the apparent velocity and overestimated or underestimated values for the apparent dispersivity were obtained, compared to the values derived by fully accounting for the actually measured tracer-input functions.

Remarkably, the 1-D CDE was capable of adapting rather well to BTCs even if strongly simplified approximations for the tracer-input function were presumed. It can be concluded that despite good agreement between a BTC and a least-squares fit of the 1-D CDE, transport parameters derived as fitting parameters can be biased if they rely on inadequate tracer-input approximations. The results therefore suggest that transport parameter estimation based on laboratory or field tracer experiments can benefit from monitoring of the tracer-input function and subsequent consideration of the measured tracer-input function in the analysis of BTCs.

Acknowledgements This work was funded by the Ruhr-University Bochum. The experiments would have been impossible without the technical support of Thorsten Gökpinar and Thomas Griese, whose assistance is gratefully acknowledged. The authors also want to thank the associate editor and two anonymous reviewers for their very instructive comments.

References

Boggs M, Young S, Beard L, Gelhar L, Rehfeld K, Adams E (1992) Field study of dispersion in a heterogeneous aquifer: 1. overview and site description. Water Resour Res 28(12):3281–3291

Brouyère S (2003) Modeling tracer injection and well-aquifer interactions: a new mathematical and numerical approach. Water Resour Res 39(3):1070. doi:10.1029/2002WR001,813

Brouyère S, Carabin G, Dassargues A (2005) Influence of injection conditions on field scale tracer experiments. Ground Water 43(3):389–400

Bulmer M (1979) Principles of statistics. Dover, Mineola, NY

Cortis A, Berkowitz B (2004) Anomalous transport in "classical" soil and sand columns. Soil Sci Soc Am J 68:1539–1548

Dagan G (1989) Flow and transport in porous formations. Springer, Heidelberg, Germany

de Barros F, Nowak W (2010) On the link between contaminant source release conditions and plume prediction uncertainty. J Contam Hydrol 116:24–34

Delleur J (1998) The handbook of groundwater engineering. Springer, Heidelberg, Germany

Diersch H (1996) Interactive, graphics-based finite element simulation system FEFLOW for modeling groundwater flow, contaminant mass and heat transport processes: user's manual version 4.5. WASY, Berlin

Drost W, Klotz D, Koch A, Moser H, Neumaier F, Rauert W (1968) Point dilution methods of investigating groundwater flow by means of radioisotopes. Water Resour Res 4(1):125–146

Englert A, Kowalsky M, Li L, Long P, Hubbard S (2007) Characterization of transient transport behavior during biostimulation field experiments using novel breakthrough analysis approaches. EOS Trans AGU 88(52), Fall Meet. Suppl., Abstract H21C-0707

Englert A, Hubbard S, Williams K, Li L, Steefel C (2009) Feedbacks between hydrological heterogeneity and bioremediation induced biogeochemical transformation. Environ Sci Technol 43(14):5197–5204

Gelhar L, Welty C, Rehfeld K (1992) A critical review of data on field-scale dispersion in aquifers. Water Resour Res 28(7):1955–1974

Hess K (1989) Use of borehole flowmeter to determine spatial heterogeneity of hydraulic conductivity and macrodispersivity in a sand and gravel aquifer, Cape Cod, Massachusetts. Paper presented at the NWWA Conference on New Field Techniques for Quantifying the Physical and Chemical Properties of Heterogeneous Aquifers, Dallas, TX, 20–23 March 1989, National Water Well Assoc., Westerville, OH

Huang K, Toride N, van Genuchten M (1995) Experimental investigation of solute transport in large, homogeneous and heterogeneous, saturated soil columns. Transport Porous Media 18:283–302

Koltermann C, Gorelick S (1996) Heterogeneity in sedimentary deposits: a review of structure-imitating, process-imitating, and descriptive approaches. Water Resour Res 32(9):2617–2658

Kreft A, Zuber A (1978) On the physical meaning of the dispersion equation and its solutions for different initial and boundary conditions. Chem Eng Sci 33:1471–1480

Leibundgut C, Maloszewski P, Külls C (2009) Tracers in hydrology. Wiley-Blackwell, Chichester, UK

Levy M, Berkowitz B (2003) Measurement and analysis of non-Fickian dispersion in heterogeneous porous media. J Contam Hydrol 64:203–226

Moench A (1989) Convergent radial dispersion: a Laplace transform solution for aquifer tracer testing. Water Resour Res 25(3):439–447

Nowak W, de Barros F, Rubin Y (2010) Bayesian geostatistical design: task-driven optimal site investigation when the geostatistical model is uncertain. Water Resour Res 46, W03535. doi:10.1029/2009WR008,312

Rolle M, Eberhardt C, Chiogna G, Cirpka O, Grathwohl P (2009) Enhancement of dilution and transverse reactive mixing in porous media: experiments and model-based interpretation. J Contam Hydrol 110:130–142

Schincariol R, Schwartz W (1990) An experimental investigation of variable density flow and mixing in homogeneous and heterogeneous media. Water Resour Res 26(10):2317–2329

Silliman S, Simpson E (1987) Laboratory evidence of the scale effect in dispersion of solutes in porous media. Water Resour Res 23(8):1667–1673

Sudicky E (1986) A natural gradient experiment on solute transport in a sand aquifer: spatial variability of hydraulic conductivity and its role in the dispersion process. Water Resour Res 22(13):2069–2082

van Beek C, Breedveld R, Juhász-Holterman M, Oosterhof A, Stuyfzand P (2009) Cause and prevention of well bore clogging by particles. Hydrogeol J 17:1877–1886

van Genuchten M, Alves W (1982) Analytical solutions for the one-dimensional convective–dispersive solute transport equation. Technical Bulletin 1661, Agricultural Research Service, USDA, Washington, DC

Vereecken H, Döring U, Hardelauf H, Jaekel U, Hashagen U, Neuendorf O, Schwarze H, Seidemann R (2000) Analysis of solute transport in a heterogeneous aquifer: the Krauthausen field experiment. J Contam Hydrol 45:329–358

Werth Y, Cirpka O, Grathwohl P (2006) Enhanced mixing and reaction through flow focusing in heterogeneous porous media. Water Resour Res 42, W12414. doi:10.1029/2005WR004,511